SAR Imaging Using Multidimensional Continuous Wavelet Transform and Applications to Polarimetry and Interferometry

E. Colin,[1,2] M. Tria,[1,3] C. Titin-Schnaider,[1] J.P. Ovarlez,[1] M. Benidir[3,4]

[1] ONERA, DEMR, BP 72, 92322 Chatillon, France

[2] University of Paris VI-Jussieu, France

[3] University of Paris XI-Orsay, France

[4] L2S, Supélec, Gif-sur-Yvette, France

Received 1 May 2004; accepted 1 November 2004

ABSTRACT: Usual SAR imaging process makes the assumption that the reflectors are isotropic and white (i.e., they behave in the same way regardless the angle from which they are viewed and the emitted frequency within the bandwidth). The multidimensional continuous wavelet transform (CWT) in radar imaging was initially developed to highlight the image degradations due to these assumptions. In this article the wavelet transform method is widened to polarimetry and interferometry fields. The wavelet tool is first used for polarimetric image enhancement, then for coherence optimization in interferometry. This optimization by wavelets, compared with the polarimetric one, gives better results on the coherence level. Finally, a combination of both methods is proposed. © 2005 Wiley Periodicals Inc. Int J Imaging Syst Technol, 14, 206–212, 2004; Published online in Wiley InterScience (www.interscience.wiley.com). DOI 10.1002/ima.20025

Key words: synthetic aperture radar; wavelets; polarimetry; Interferometry

I. INTRODUCTION

The radar imaging process (Mensa, 1981; Carrara et al., 1995) consists in calculating a complex backscattering function $H(\vec{k})$ collected by a moving radar and in forming the spatial repartition $I(\vec{r})$ of the bright scatterers which reflect a part of the emitted radar signal. The square modulus of $H(\vec{k})$ is the radar cross section (RCS) of the object. It is expressed in square meters. The wave vector $\vec{k}$ expresses as

$$\vec{k} = \frac{2f}{c}\begin{pmatrix}\cos(\theta)\cos(\psi)\\ \sin(\theta)\cos(\psi)\\ \sin(\psi)\end{pmatrix}$$

where f is the frequency, c is the speed of light, θ is the azimuthal aspect angle, and ψ the elevation look angle.

Correspondence to: E. Colin or M. Tria; e-mail: colin@onera.fr; tria@onera.fr

For simplification, we consider the scenario presented in Figure 1 and often accepted in the literature (Gough and Hawkins, 1997; Soumekh, 1994, 1999): the moving aircraft (which carries the radar) is supposed to be in the same plane (X, Y) that the ground zone containing the illuminated object $(\psi = 0)$. The wave vector becomes

$$\vec{k} = \frac{2f}{c}\begin{pmatrix}\cos(\theta)\\ \sin(\theta)\end{pmatrix},$$

with $k = |\vec{k}| = \frac{2f}{c}$ and $\theta = \arg(\vec{k})$.

SAR imaging processes generally assume that the sensor has a fixed orientation with respect to the object and emits a fixed wave frequency. However, if the object is illuminated with a broadband signal and a large angular extent, one can reasonably think that the amplitude of the backscatterers depends on the frequency and the aspect angle. Considering this amplitude variation, the spatial repartition of reflectors $I(\vec{r})$ must depend on the wave vector $\vec{k}$ and must now be noted $I(\vec{r},\vec{k})$. This quantity is called "extended images" relative to $I(\vec{r})$. It can be rewritten $I(\vec{r},k) \equiv I(x,y;f,\theta)$, where $(x,y;f,\theta)$ are respectively the range, the cross-range, the frequency and the illumination aspect angle.

The multidimensional wavelet transform for SAR imaging has been performed to build such hyperimages $I(\vec{r},\vec{k})$ in order to highlight the frequency and the angular energetic repartition of the reflectors (Potter et al., 1995; Potter and Moses, 1997; Ovarlez et al., 2003; Tria et al., 2004). A different interpretation of these hyperimages allows us to consider the images $I(x,y;f_o,\theta_o)$ of the illuminated scene for each emitted frequency f_o and for each aspect angle θ_o (Ovarlez et al., 2003).

In this article, the purpose is to use the wavelet tool on polarimetric and interferometric SAR images. Interferometry provides information on the target height by using the signal of two antennas.

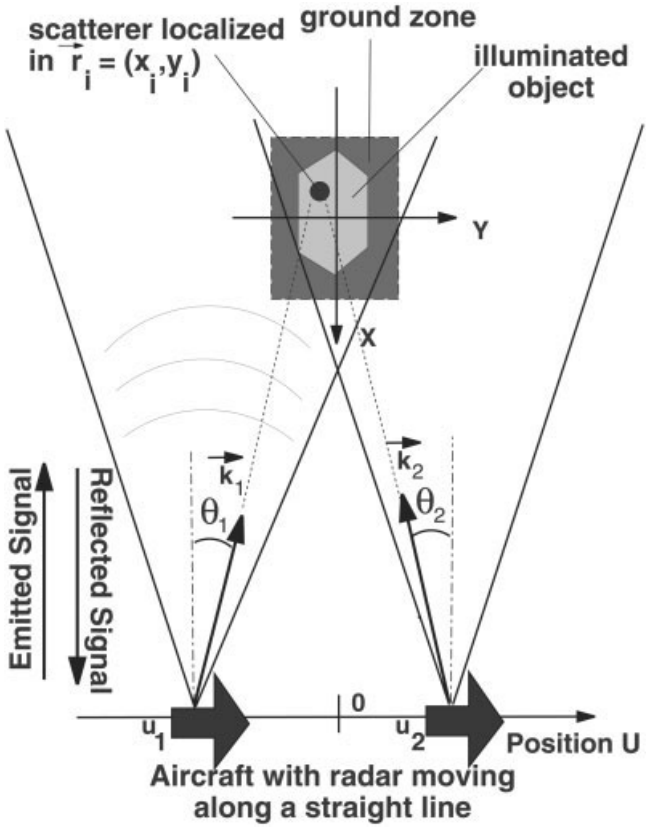

Figure 1. A reflector, viewed at two different illumination angles in SAR-stripmap mode (the aircraft and the ground zone are supposed to be in the same plane).

The polarimetry analyzes physical scattering properties of the imaged media, transmitting and receiving microwave radiation that is either horizontally (H) or vertically (V) polarized. Using the wavelet tool, the polarimetric parameters and the interferometric coherence can be calculated for each aspect angle and for each emitted frequency. The study consists in finding the aspect angle and the frequency that give the more convenient parameter for a better target recognition or target height estimation (Tria and Colin, 2004).

The next section is devoted to the construction of the extended radar images $I(\vec{r},\vec{k})$ using time-frequency analysis and the physical group theory. These images $I(\vec{r},\vec{k})$ represent, in fact, the energy distribution of the backscattering function $H(\vec{k})$ in the hyperplane $(\vec{r},\vec{k})$. General distributions based on a hermitian and bilinear form of the backscattering function $H(\vec{k})$ are first built. Then, to overcome some drawbacks generated by this construction, we focus on the construction of regularized distributions that will introduce the wavelet transform.

EXTENDED RADAR IMAGING

Time-frequency analysis and physical group theory allow us to build extended radar images (Bertrand and Bertrand, 1996; Bertrand et al., 1991; 1994; Ovarlez et al., 2003). The dimension of these images, called hyperimages, is the product of the dimension of the vector $\vec{r}$ by the dimension of the vector $\vec{k}$.

The principle of the extended radar imaging (Bertrand et al., 1994) is based on a physical group of transformations, the similarity group S. This group acts on the physical variables $\vec{r}$ and $\vec{k}$ by rotations $\mathcal{R}_\theta$, dilations a in length (or time), and translations θ according to

$$\begin{array}{ccc} \vec{r} & \to & \vec{r}\,' = a\mathcal{R}_\theta\vec{r} + \delta\vec{r} \\ \downarrow & & \downarrow \\ \vec{k} & \to & \vec{k}\,' = a^{-1}\mathcal{R}_\theta\vec{k}. \end{array} \tag{1}$$

The transformation law of the backscattering function $H(\vec{k})$, and its extended image $I(\vec{r},\vec{k})$, is therefore given by

$$\begin{array}{ccc} H(\vec{k}) & \to & H'(\vec{k}) = a' e^{-2i\pi\vec{k}\cdot\delta\vec{r}} H(a\mathcal{R}_\theta^{-1}\vec{k}) \\ \downarrow & & \downarrow \\ I(\vec{r},\vec{k}) & \to & I'(\vec{r},\vec{k}) = I(a^{-1}\mathcal{R}_\theta^{-1}(\vec{r}-\delta\vec{r}), a\mathcal{R}_\theta^{-1}\vec{k}). \end{array} \tag{2}$$

General Formulation of the Extended Images. To build the energy distribution $I(\vec{r},\vec{k})$, a first approach consists in representing it as a Hermitian and bilinear form of the backscattering function $H(\vec{k})$:

$$I(\vec{r},\vec{k}) = \int\int K(\vec{k}_1,\vec{k}_2;\vec{r},\vec{k}) H(\vec{k}_1) H^*(\vec{k}_2) d\vec{k}_1 d\vec{k}_2, \tag{3}$$

where the kernel $K(\vec{k}_1,\vec{k}_2;\vec{r},\vec{k})$ is supposed to be Hermitian. This kernel is not known but can be determined with some physical constraints made on the distribution $I(\vec{r},\vec{k})$:

- The distribution can satisfy the property of covariance by the similarity group $\mathcal{S}$ given by (2).
- The distribution $I(\vec{r},\vec{k})$ can be seen, in $\mathcal{R}^2$, as a spatial density (for a given k). Then, the distribution has to be positive. Its integral on some surface $\mathcal{D}$ can therefore be interpreted as the RCS contribution $\sigma'_{\mathcal{D}}(\vec{k})$ of all the reflectors contained in $\mathcal{D}$:

$$\sigma_{\mathcal{D}}(\vec{k}) = \int_{\mathcal{D}} I(\vec{r},\vec{k}) d\vec{r}. \tag{4}$$

- If $\mathcal{D}$ represents the whole plan, the distribution can respect the well-known marginal property:

$$\int I(\vec{r},\vec{k}) d\vec{r} = \left| H(\vec{k}) \right|^2. \tag{5}$$

- The energy conservation between the distribution space and the backscattering function leads to an important relation (Moyal formula) that connects the inner product between two given complex backscattering functions, H_1 and H_2, and their associated distributions, I_1 and I_2:

$$\left| \int H_1(\vec{k}) H_2^*(\vec{k}) d\vec{k} \right|^2 = \int\int I_1(\vec{r},\vec{k}) I_2^*(\vec{r},\vec{k}) d\vec{r} d\vec{k} \tag{6}$$

Time-frequency analysis has shown that no distribution can satisfy all these properties. For example, the property (6) does not always allow us to obtain a distribution everywhere positive, which is inconsistent with the RCS nature of the distribution given by (4) or (5).

To overcome this drawback, it is possible to build a regularized form of these distributions obtained by smoothing the general distribution given by (3). These regularized distributions verify the constraints (2), (4), and (6) but not the marginalization property (5). The construction of these extended images, which introduces the wavelet transform, is developed in the next section.

a) polarimetric RGB composition reference image
red=s_1, green=s_2, blue=s_3 (see Eq. 14)

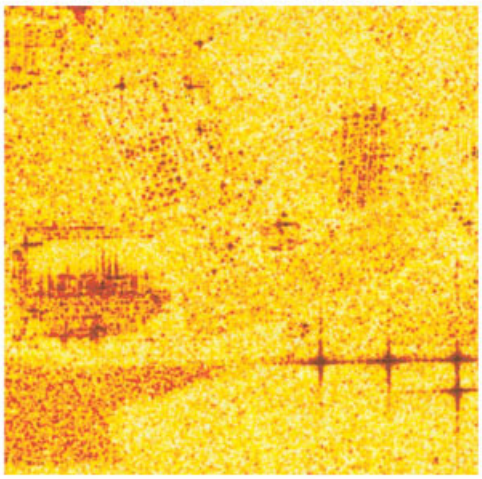

b) H (classical)

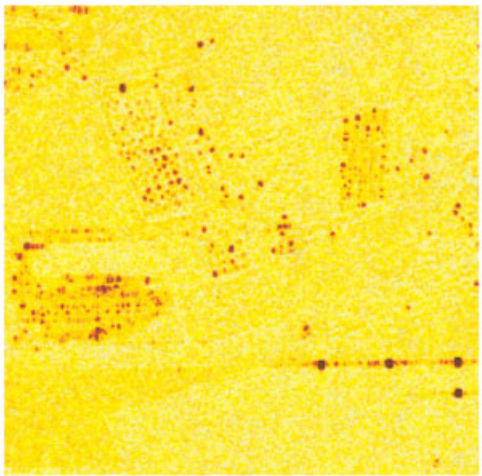

c) $H_{\max}$

Figure 2. Comparison between H and $H_{\max}$.

Construction of the extended images by the continuous wavelet transform. Let $\phi(k, \theta)$ be a mother wavelet supposed to represent the complex backscattering function of a reference target. The associated energetic distribution $I_\phi(\vec{r}, \vec{k})$ in the hyperplane $(\vec{r}, \vec{k})$ is supposed to be well located around the spatial origin $\vec{r} = \vec{0}$ and $(k, \theta) = (1, 0)$. Here a two-dimensional separable Gaussian function is used:

$$\phi(k, \theta) = e^{-(k-1/\sigma_k)^2} \cdot e^{-(\theta/\sigma_\theta)^2},$$

where the two free parameters σ_k and σ_θ control the spread in frequency and in angular domain and play on interrelated resolutions in spatial domain $\vec{r} = (x, y)$, frequency, and angle.

By the action of the group $\mathcal{S}$, a family of wavelets $\Psi_{\vec{r}_0,\vec{k}_0}(\vec{k})$ can be generated from the mother wavelet $\phi(k, \theta)$ according to

$$\begin{aligned}\Psi_{\vec{r}_0,\vec{k}_0}(\vec{k}) &= \frac{1}{k_0} e^{-2i\pi\vec{k}\cdot\vec{r}_0} \phi\left(\frac{1}{k_0}\mathcal{R}_{\theta_0}^{-1}\vec{k}\right) \\ &= \frac{1}{k_0} e^{-2i\pi\vec{k}\cdot\vec{r}_0} \phi\left(\frac{k}{k_0}, \theta - \theta_0\right). \end{aligned} \tag{7}$$

A regularized distribution $\tilde{I}(\vec{r}_0, \vec{k}_0)$ can be built by smoothing the general distribution $I(\vec{r}, \vec{k})$ given by (3).

Using Moyal formula (6), covariance property (2), and taking $H_1(\vec{k}) = H(\vec{k}), H_2(\vec{k}) = \Psi_{\vec{r}_0,\vec{k}_0}(\vec{k}), I_1 = I_H$, and $I_2 = I_\phi$, we obtain:

$$\begin{aligned}\tilde{I}(\vec{r}_0, \vec{k}_0) &= \iint I_H(\vec{r}, \vec{k}) \\ &\quad \times I_\phi^*\left(k_0\mathcal{R}_{\theta_0}^{-1}(\vec{r} - \vec{r}_0), \frac{1}{k_0}\mathcal{R}_{\theta_0}^{-1}\vec{k}\right) d\vec{r}\,d\vec{k} \\ &= \left| \int H(\vec{k}) \frac{1}{k_0} e^{-2i\pi\vec{k}\cdot\vec{r}_0} \phi*\left(\frac{1}{k_0}\mathcal{R}_{\theta_0}^{-1}\vec{k}\right) d\vec{k} \right|^2. \end{aligned} \tag{8}$$

The right-hand side is nothing but the wavelet coefficient $C(\vec{r}_0, \vec{k}_0)$; which is introduced as the invariant scalar product of the similarity group $\mathcal{S}$ between the backscattering function H and each element $\Psi_{\vec{r}_0,\vec{k}_0}$ of the wavelet basis:

$$\begin{aligned}C(\vec{r}_0, \vec{k}_0) &= \int H(\vec{k}) \Psi^*_{\vec{r}_0,\vec{k}_0}(\vec{k}) d\vec{k} \\ &= \int_0^{2\pi} d\theta \int_0^{+\infty} kH(k, \theta) \Psi^*_{\vec{r}_0,\vec{k}_0}(\vec{k}) dk. \end{aligned} \tag{9}$$

The reconstruction property allows us to recover the signal with the knowledge of its wavelet coefficients:

$$H(\vec{k}) = \frac{1}{\kappa(\phi)} \int d\vec{r}_0 \int C(\vec{r}_0, \vec{k}_0) \Psi_{\vec{r}_0,\vec{k}_0}(\vec{k}) d\vec{k}_0, \tag{10}$$

where $\kappa(\phi)$ is the admissibility coefficient defined as

$$\kappa(\phi) = \int \frac{|\phi(\vec{k})|^2}{k^2} d\vec{k} < \infty. \tag{11}$$

1. Interpretation of the hyperimages $I(\vec{r}, \vec{k})$. Let us rewrite $I(\vec{r}, \vec{k}) \equiv I(x, y; f, \theta)$. For each frequency f_o and each aspect angle $\theta_o, I(x, y; f_o, \theta_o)$ represents the spatial repartition of reflectors that respond at this frequency and this angle. Inversely, for each reflector located at $\vec{r}_o = (x_o, y_o)$, we can extract its energetic feature $I(x_o, y_o;\ f, \theta)$ as a function of frequency f and aspect angle θ.

To analyze this 4D structure, a visual display interface called i4D (Castelli and Bobillot, 1997). has been developed and allows to carry out an interactive and dynamic analysis.

2. Extension to polarimetry and interferometry. The extension to polarimetric and interferometric fields is possible by exploiting the complex wavelet coefficients $C(\vec{r},\vec{k})$ defined previously. Indeed, the quantity $C(x,y;f_o,\theta_o)$ can be considered as a complex image corresponding to the emitted frequency f_o and the aspect angle θ_o. These wavelet coefficients are calculated in the same way for each interferometric antenna and for each polarization emission and reception couple. In the following, a 500 × 500 pixel image [see Fig. 2(a)] has been selected from the airborne RAMSES X-band data at Bretigny (Boutry, 1996). It contains industrial buildings, trees, a parking lot, and four canonical trihedrons used for calibration. Wavelet coefficients $C(x,y,f,\theta)$ have been calculated for 10 angles θ_0 and 10 frequencies f_0.

The parameters (σ_k,σ_θ), introduced previously in the Gaussian mother wavelet, determine, respectively, the frequency and angular bandwidths δk and $\delta\theta$ of the mother wavelet $\phi(k,\theta)$ and thus control the frequency and angular spread of the wavelets $\Psi_{\vec{r}_0,\vec{k}_0}(\vec{k})$.

The bandwidths δk and $\delta\theta$ are defined as the 3-dB pass-band (also called root mean-square bandwidth) (Mallat, 1998). This 3-dB pass-band definition is related in the figure (3).

Denoting $k_1 = 1$ as the reference frequency, the 3-dB pass-band δk in the frequency domain is defined such that

$$\frac{|\phi(k_1 \pm \frac{\delta k}{2})|^2}{|\phi(k_1)|^2} = 0.5. \tag{12}$$

The angular bandwidth $\delta\theta$ is defined in the same way with the reference angle $\theta_1 = 0$.

$\delta\theta$ has been chosen to obtain an angular spread of the wavelets equal to 30% of the total angular extend $\Delta\theta$ covered by the radar. δk has been chosen to obtain a frequency spread of the wavelets localized at the central frequency $k = k_c$, equal to 30% of the total emitted bandwidth signal Δk (see Fig. 3).

POLARIMETRY

A full polarimetric radar is designed to transmit and receive microwave radiation that is horizontally polarized (H) or vertically polarized (V). It contains the whole information upon the electromagnetic mechanisms met by waves. The polarimetric generalization of the backscattering coefficient is called the scattering matrix $\mathcal{S}$. The matrix is composed of four complex numbers, representing the complex backscattering coefficients for all four polarization combinations, hH, hV, vH, and vV (capital letters indicate the transmit wave polarization and small letters the received polarization):

$$S = \begin{pmatrix} S_{\mathrm{bH}} & S_{\mathrm{hV}} \\ S_{\mathrm{vH}} & S_{\mathrm{vV}} \end{pmatrix}. \tag{13}$$

The purpose of the polarimetric analysis is to separate and identify these mechanisms with the objective to discriminate and recognize targets. Several sets of parameters are available to analyze the distributed targets (Titin-Schnaider, 1999). Under the reciprocity assumption framework, i.e., $S_{\mathrm{vH}} = S_{\mathrm{Vh}}$, the three component scattering vector $\vec{s}$ is used instead of the scattering matrix for each pixel (x, y):

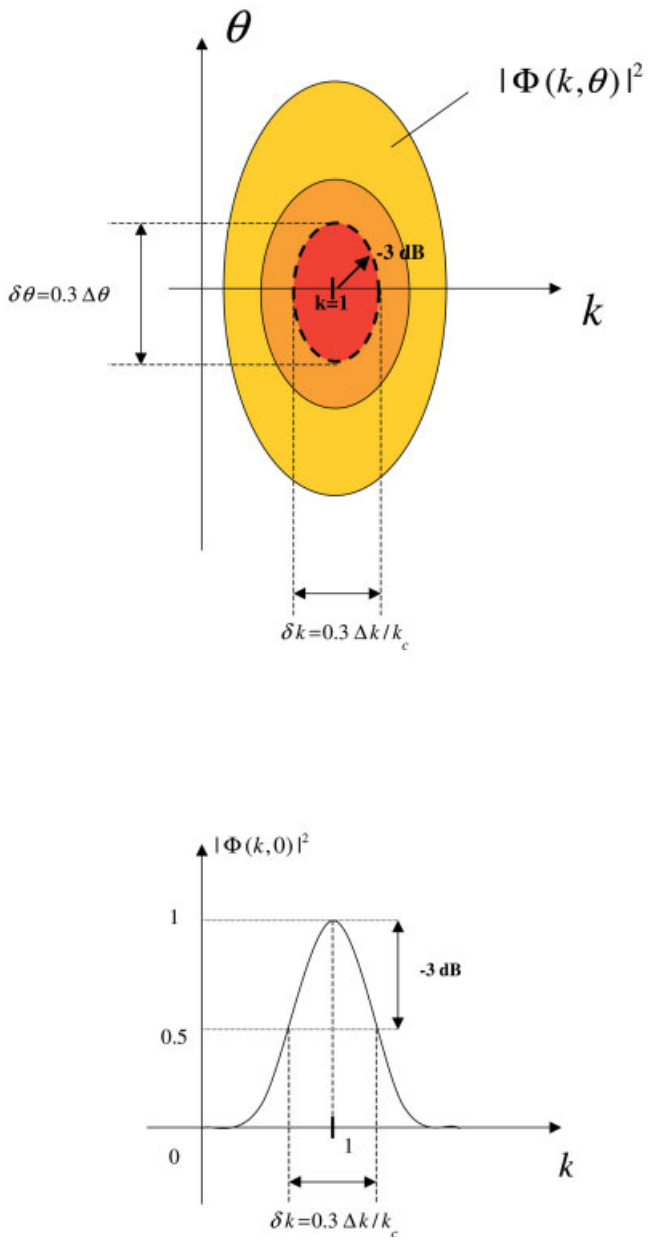

Figure 3. The frequency and angular bandwidths of the mother wavelet $\phi(k, \theta)$ defined in the sense of the 3-dB pass-band. [Color figure can be viewed in the online issue, which is available at www.interscience.wiley.com.]

$$\vec{s}(x,y) = \begin{pmatrix} s_1 \\ s_2 \\ s_3 \end{pmatrix} = \frac{1}{\sqrt{2}} \begin{pmatrix} S_{\mathrm{hH}} + S_{\mathrm{vV}} \\ S_{\mathrm{hH}} - S_{\mathrm{vV}} \\ 2S_{\mathrm{hV}} \end{pmatrix}. \tag{14}$$

Then the coherency matrix from which all polarimetric parameters sets can be deduced, is written:

$$T(x,y) = \langle \vec{s}(x,y), \vec{s}(x,y) \rangle. \tag{15}$$

The wavelet tool allows us to calculate a diffusion vector $\vec{s}$ for each angle and each frequency: $\vec{s}(x,y;f,\theta)$. All polarimetric parameters can be then expressed in function of the coherency matrix $T(x,y;f,\theta)$ and then are also obtained for each angle and each frequency. A key polarimetric parameter used to distinguish natural targets from

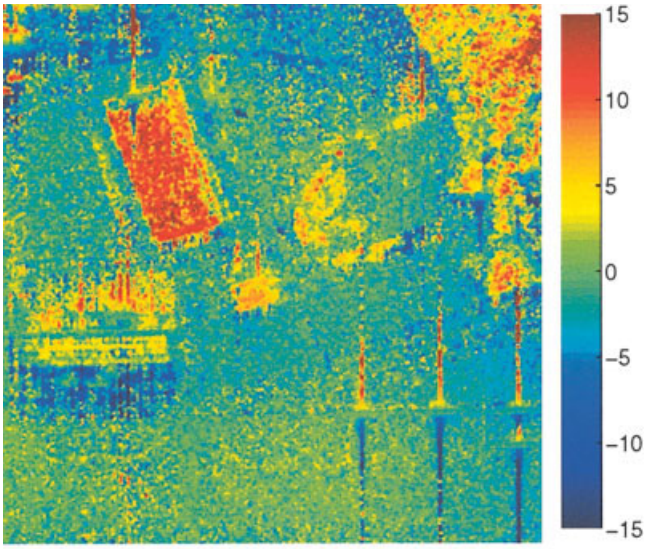

a- initial Elerahan (meters) in vV polarization

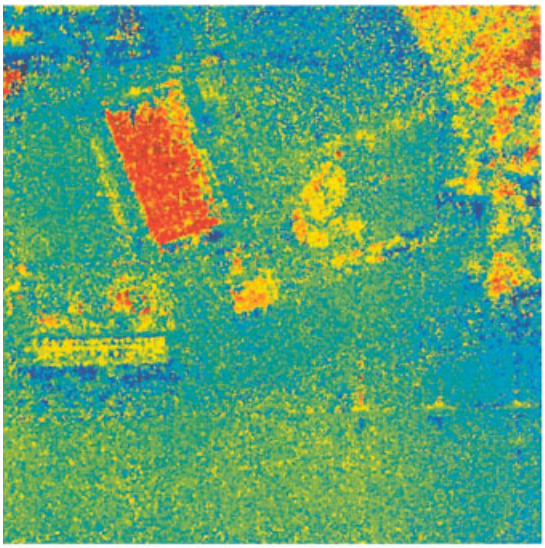

b- after polarimetric optimization

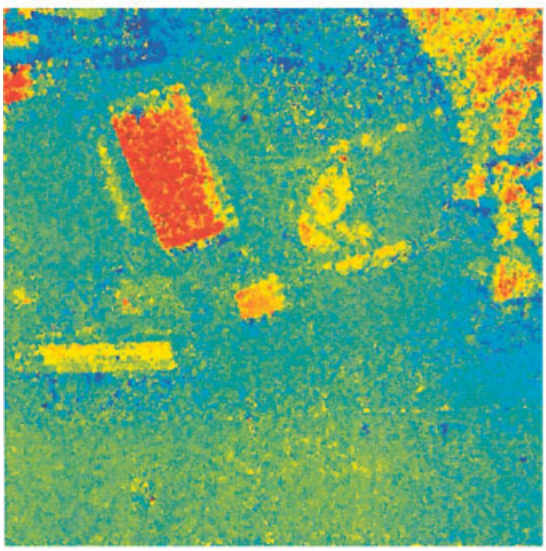

c- after time-frequency optimization

Figure 4. Elevation map obtained from interferometric angle. (a) In polariazation vV. (b) After polarimetric optimization. (c). After time-frequency optimation.

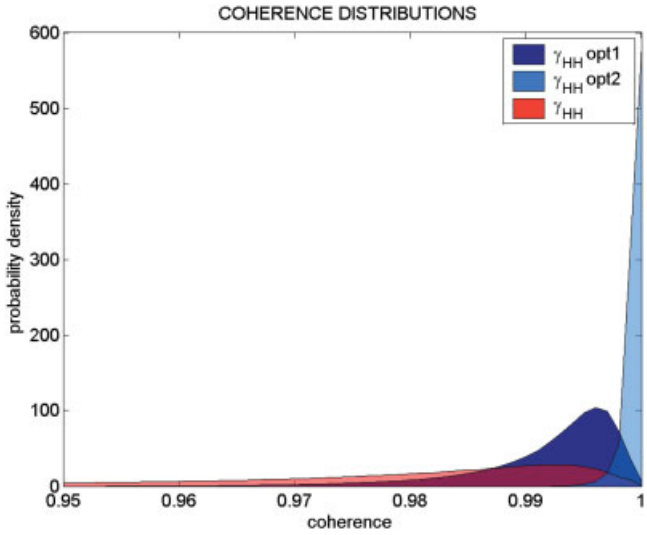

Figure 5. Comparison of the coherence distributions; opt1 is the polarimetric optimization and opt2 is the time-frequency optimization. [Color figure can be viewed in the online issue, which is available at www.interscience.wiley.com.]

artificial one as buildings is entropy H: This is a formal measure of the randomness of the scattering features in the scene. By definition

$$H = -\sum_{i=1}^{3} p_i \log_3(p_i), p_i = \frac{\lambda}{\lambda_1 + \lambda_2 + \lambda_3}, \tag{16}$$

where λ_i are the eigenvalues of the matrix T. When the entropy is low, we have scattering from a single object (a smooth surface, for instance), whereas when the entropy is high, we have volume scattering from vegetation. This information can be used to provide automatic classification of radar scenes. Using the diffusion vector $\vec{s}(x, y; f, \theta)$, entropy images can be calculated for each frequency and each angle. To improve target enhancement, an image of minimal and maximal entropy can be obtained, defined as

$$H_{\max}(x, y) = \max_{\theta, f} H(x, y, f, \theta) \tag{17}$$

$$H_{\min}(x, y) = \min_{\theta, f} H(x, y, f, \theta). \tag{18}$$

Those images show that the "maximal entropy" allows us separate deterministic targets as buildings better than initial entropy [Fig. 2(b) and 2(c)]. On the contrary, $H_{\min}$, giving a very low entropy on the whole image, is not interesting for contrast enhancement.

INTERFEROMETRY

Interferometry is an efficient tool when used to obtain the topography of a given area. It is based on the measurement of the phase difference between two paired pixels of two complex SAR images, obtained from the data collected by two antennas. The target elevation is proportional to this phase difference, known as interferometric phase. If s_1 is the scattering coefficient for a pixel of the first image, and s_2 is the coefficient for the same pixel obtained from the

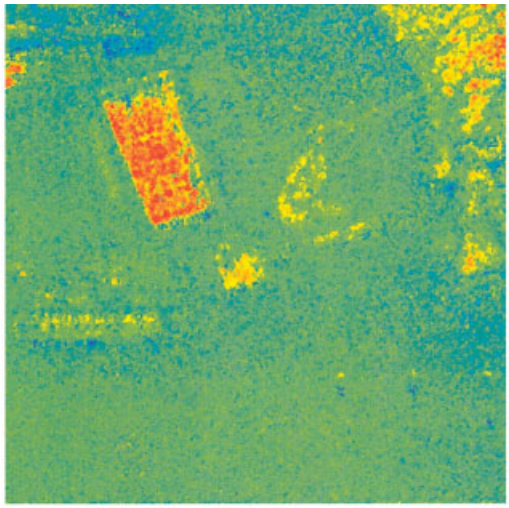

a-coherence first optimized with wavelets, then with polarimetry

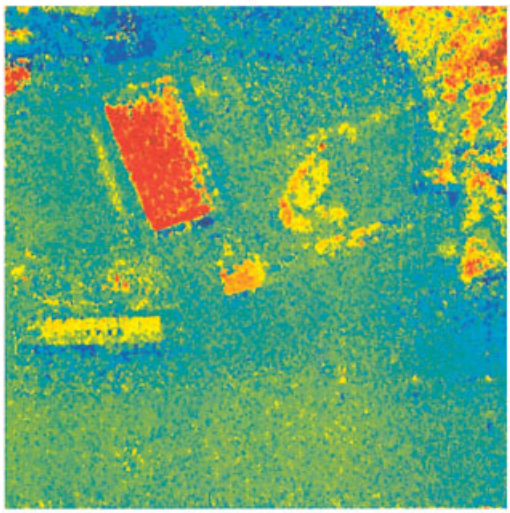

b-coherence computation performed after wavelet coefficients average, then optimized with polarimetry

Figure 6. Elevation map obtained from interferometric angle after two different methods combining polarimetric and time-frequency information.

second image, the coherence of the pixel is mathematically defined as

$$\gamma = \frac{\langle s_1 s_2^* \rangle}{\sqrt{\langle s_1 s_1^* \rangle}\sqrt{\langle s_2 s_2^* \rangle}} \tag{19}$$

The interferometric coherence calculus requires averaging over many samples from the same distribution. Computationally, it is estimated using a boxcar filter where samples are in a $N \times N$ window. We choose here $N = 3$,

$$\gamma = \frac{\sum_{i=1}^{N\times N} s_1(i) s_2^*(i)}{\sqrt{\sum_{i=1}^{N\times N} |s_1(i)|^2 \sum_{i=1}^{N\times N} |s_2(i)|^2}} \tag{20}$$

The phase of γ is the interferometric phase, and its modulus is called coherence. It is known that the height estimation is all the more reliable as the coherence is large.

One possible use of the wavelet tool is the coherence optimization possibility, and consequently and increase of the accuracy of the reconstructed elevation profiles for each scatterer. Interferometric phase can be computed for each angle and each frequency. For each pixel, we find a couple (f_o, θ_o) giving the maximum coherence. Then the interferometric phase ϕ corresponding to this couple (f_o, θ_o) is used to calculate the elevation map, using the relation.

$$h = \frac{\Phi}{2\pi} e_a \tag{21}$$

where e_a is the "ambiguity height" and depends on the geometric configuration of the radar and on the range of the target.

This method of optimization is called the "time-frequency optimization." Results are compared with those obtained after the optimization coherence polarimetry (Colin et al., 2004) on Figure 4. There are commented on in the following section.

IFPOL

One of the benefits that result from the combination of polarimetric and interferometic data is the coherence optimization using polarimetric data. That is why we first compare results of the time-frequency optimization with those of the polarimetric optimization.

There are several procedures to extend the definition of the interferometric coherence to polarimetry. The first on (Cloude and Papa thanassiou, 1998) is to define two vectors, called "mechanism," on which the scattering vectors $\vec{s}_1$ and $\vec{s}_2$ are projected. The second one is a restriction of the first definition: only one "mechanism" is defined, the same for both antennas (Colin et al., 2004). The last method restricts the choice of the mechanism to an elliptic polarization for emission and reception (Pascula et al., 2000). The second method described in (Colin et al., 2004) has been chosen here, because it is gives the best results on the interferometric phase on this data set, while reaching the same level of coherence. Results of the comparison between this polarimetric optimization with the time-frequency optimization are shown in Figure 4. The quality of the interferometric angles is similar from image b to image c. However, coherence modulus is better optimized with the time-frequency optimization than with polarimetric optimization, as shown on coherence modulus distributions in Figure 5. The distributions are calculated on the 500×500 pixels of the whole image and then are normalized.

The coherence time-frequency optimization wavelet is performed for a given polarization, without using the polarimetric information. One way to combine this optimization with the polarimetric one is to perform them successively. In Figure 6(a), the time-frequency optimization has been first applied to the three scattering vector components, then the polarimetric optimization has been performed. This method, which will be called "method a," gives a very smoothed image, each optimization requiring an additional average to calculate the coherence. The drawback of this is that samples used to compute the coherence can be finally chosen in heterogeneous areas. This leads with our data, to an underestimated height on buildings.

Table I. Height estimation of three buildings using methods a and b.

Estimated heights, m	Building 1	Building 2	Building 3
Method a	8.3	1.0	4.5
Method b	10.6	3.4	7.1
Ground truth	11.5	3.5 to 7	10

To avoid this problem, another idea is to use the polarimetric optimization after an average performed on all wavelet coefficients of the pixel:

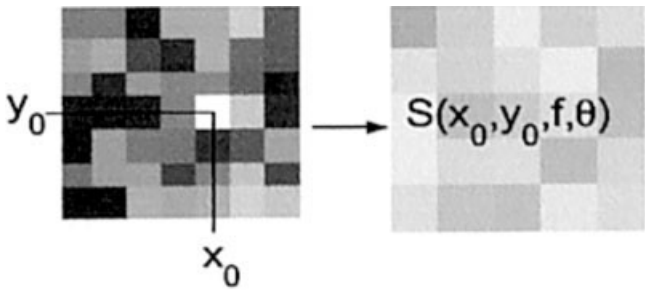

$$\gamma = \frac{\sum_{(f,\theta)=1}^{n_f \times n_\theta} s_1(f,\theta) s_2^*(f,\theta)}{\sqrt{\sum_{(f,\theta)=1}^{n_f \times n_\theta} |s_1(f,\theta)|^2 \sum_{(f,\theta)=1}^{n_f \times n_\theta} |s_2(f,\theta)|^2}} \qquad (22)$$

This method, called "method b" [Fig 6(b)], leads to results very similar to those obtained with time-frequency optimization alone [Fig 4(c)].

The estimated heights of three buildings are listed in the Table I.

CONCLUSIONS

A Wavelet tool applied to polarimetry and interferometry seems to be an additional method to improve target enhancement and height estimation.

Concerning interferometry, the major difficulty of the coherence optimization methods is the choice of the samples used to compute the coherence: classical interferometry requires a choice of several pixels (x, y) to compute the coherence; time-frequency 4D coefficients allow us to use samples either in (x, y) domain or in (f, θ) domain. However, both polarimetric and time-frequency coherence definitions lead to a deterioration of the image resolution. This article has proposed and compared two different methods to combine the polarimetric and time-frequency optimization. In the future, other efforts could be made to remedy to these limitations, and to determine the more convenient optimization.

We can also discuss the utility of adaptative wavelets: the idea is to constuct wavelets with different parameter couples $(\sigma_k, \sigma_\theta)$, whose choice is a function of the analyzed zone in the image. For example, the parameter could be different for artificial targets (buildings) and for natural targets (soil, vegetation). This distinction between artificial and natural targets could be made by separating the low entropy from the high entropy areas. The objective will be to study the effects of such adaptative wavelets on the quality of the thus-constructed images.

REFERENCES

J. Bertrand and P. Bertrand, The concept of hyperimage in wide-band radar imaging, IEEE Trans Geosci Remote Sens, 34 (1996), 1144–1150.

J. Bertrand, P. Bertrand, and J.P. Ovarlez, Dimensionalized wavelet transform with application to radar imaging, Proc IEEE-ICASSP (May 1991), Toronto, Canada.

J. Bertrand, P. Bertrand, and J.P. Ovarlez, Frequency directive scanning in laboratory radar imaging, Int J Imaging Syst Techno 5 (1994), 39–51.

J.M. Boutry, ONERA airborne SAR facilities, 2nd International Airborne Remote Sensing Conference, San Francisco, CA, June 1996.

W.G. Carrara, R.S. Goodman, and R.M. Majewski, Spotlight synthetic aperture radar, Artech House, Boston, London,1995.

J.C. Castelli and G. Bobillot, I4D: A new approach to RCS imaging analysis, Proc AMTA (Nov. 1997), Boston, MA.

S.R. Cloude and K.P Papathanassiou, Polarimetric SAR interferometry, IEEE TGRS 36(5) (1998).

E. Colin, C. Titin-Schnaider, and W. Tabbara, Investigation on diffferent IFPOL coherence optimization methods, presented at *POLINSAR*, Jan. 2003. [Online]. Available: http://earth.esa.int/workshops/polinsar2003/participants/colin75/

P.T. Gough and D.W. Hawkins, Unified framework for modern synthetic aperture imaging algorithms, Int J Imaging Syst and Techno 8 (1997), 343–358.

S. Mallat, Wavelet tour of signal processing, Academic Press, San Diego; 1998.

D.L. Mensa, High resolution radar imaging, Artech House, Dedham, MA, 1981.

J.P. Ovarlez, L. Vignaud, J.C. Castelli, M. Tria, and M. Benidir, Analysis of SAR images by multidimensional wavelet transform, IEE Proc Radar, Sonar, 150(4) (2003), 234–241.

C. Pascula, E. Gimena, Nieves, and J.M. Lopez-Sanchez, The equivalence between the polarisation subpace method (PSM) and the coherence optimization in polarimetric radar interferometry, EUSAR 2000, Munich, Germany.

L.C. Potter, D.M. Chiang, R. Carrire, and M.J. Gerry, A geometrical theory of diffraction (GTD)-based parametric model for radar sattering, IEEE Trans Antennas Propagat 43 (1995), 1058–1067.

L.C. Potter and R.L. Moses, Attributed scattering centers for SAR ATR, IEEE Trans Image Process 6 (1997), 79–91.

M. Soumekh, Fourier array imaging, PTR Prentice-Hall, Englewood Cliffs, UJ, 1999.

M. Soumekh, Synthetic aperture radar signal processing, John Wiley, New York, 1999.

C. Titin-Schnaider,Discriminating polarimetric parameters for radar images analysis, Proc IGARSS'99 (June 28–July 02, 1999), Hamburg.

E. Colin and M. Tria, SAR imaging using multidimensional continuous wavelet transform and applications to polarimetry and interferometry, Radar 2004, International Conference on Radar Systems, Toulouse, France, October 2004.

M. Tria, J.P Ovarlez, L. Vignaud, J.C. Castelli, and M. Benidir, SAR imaging using multidimensional continuous wavelet transform, Radar 2004, International Conference on Radar Systems, Toulouse, France, October 2001.